Published online 28 June 2011

Nucleic Acids Research, 2011, Vol. 39, No. 17 ***e114***
doi:10.1093/nar/gkr499

Emulsified BMVC derivative induced filtration for G-quadruplex DNA structural separation

Yu-Lin Tsai[1,2], Zi-Fu Wang[1,2], Wei-Wen Chen[2,3] and Ta-Chau Chang[1,2,3,*]

[1]Department of Chemistry, National Taiwan University, [2]Institute of Atomic and Molecular Sciences, Academia Sinica, Taipei 10617, Taiwan and [3]Institute of Biophotonics, National Yang-Ming University, Taipei 11221, Taiwan, Republic of China

Received March 9, 2011; Revised May 13, 2011; Accepted June 2, 2011

ABSTRACT

A novel method based on emulsion/filtration is introduced for G-quadruplex DNA structural separation. We first synthesized a lipophilic analogue of BMVC, 3,6-Bis(1-methyl-4-vinylpyridinium)-9-(12′-bromododecyl) carbazole diiodide (BMVC-12C-Br), which can form an oil-in-water (o/w) phase emulsion. Due to the binding preferences of BMVC-12C-Br emulsion to some specific DNA structures, the large emulsion (~2 μm) bound DNA was separated from the small free DNA in the filtrate by a 0.22 μm pore size MCE membrane. This method is able to isolate the non-parallel G-quadruplexes from the parallel G-quadruplexes and the linear duplexes from both G-quadruplexes. In addition, this method allows us not only to determine the absence of the parallel G-quadruplexes of $d(T_2AG_3)_4$ and the presence of the parallel G-quadruplexes of $d(T_2AG_3)_2$ in K^+ solution, but also to verify structural conversion from antiparallel to parallel G-quadruplexes of $d[AG_3(T_2AG_3)_3]$ in K^+ solution under molecular PEG condition. Moreover, this emulsion can separate the non-parallel G-quadruplexes of $d(G_3CGCG_3AGGAAG_5CG_3)$ monomer from the parallel G-quadruplexes of its dimer in K^+ solution. Together with NMR spectra, one can simplify the spectra for both the free DNA and the bound DNA to establish a spectrum-structure correlation for further structural analysis.

INTRODUCTION

A large number of guanine rich DNA sequences found in the human genome can readily form G-quadruplex (G4) structures (1–3). Recently, the biological implications of G-quadruplexes in telomeres and gene promoter regions have attracted much attention (4–8). Human telomere contains thousands of hexameric repeated TTAGGG/CCCTAA duplexes and a 100–200 nt single-stranded G-rich 3′-overhang. Of interest is that this single-stranded G-rich sequence can adopt G4 structures under certain physiological conditions. Given that the majority of cancers cause telomerase activation for telomere length maintenance (9) and the G4 structure is not a template for telomerase (10), such a structure has potential in the development of telomerase inhibitors and anti-cancer agents (11–14).

In the human BCL-2 (B-cell/lymphoma-2) gene promoter region, Hurley *et al.* (15) found that the middle four consecutive G-tracts of the BCL-2 gene promoter, ($G_3CGCG_3AGGAAG_5CG_3$) (bcl2mid), is likely to form the G4 structure in K^+ solution. BCL-2 is an oncoprotein that plays an essential role in regulating apoptosis. Aberrantly overexpressed BCL-2 is found in a number of human cancers, such as B-cell and T-cell lymphomas (16), breast (17), prostate (18), cervical (19), colorectal (20) and lung carcinoma (21). The control of BCL-2 expression provides a promising approach to cancer treatment (22–24), because the G4 structure may act as steric block to the transcription machinery. G-quadruplexes are an attractive subject for research, not only because of their relevance to the development of new anti-cancer drugs but also to explore their potential biological roles (25–27).

The G-rich sequences can form a variety of structures and may coexist in mixtures. For example, NMR analysis shows that the human telomeric sequence, $AG_3(T_2AG_3)_3$ (HT22), forms an antiparallel basket G4 structure in Na^+ solution (28), while X-ray crystallography shows that HT22 forms a parallel propeller G4 structure in the presence of K^+ (29). NMR results also suggest the presence of multiple conformers of HT22 in K^+ solution, which poses a problem for structural analysis (30). Although the propeller G4 structure is not a major structure in K^+ solution, the predominant non-parallel G4 structures in K^+ solution convert to the parallel G4

*To whom correspondence should be addressed. Tel: +1 8862 2366 8231; Fax: 8862 2362 0200; Email: tcchang@po.iams.sinica.edu.tw

structures under molecular PEG conditions (31). Similarly, NMR studies suggest the presence of multiple conformers of bcl2mid in K^+ solution (32).

Recently, gel assays have revealed that a major component of the bcl2mid monomer exists at low [K^+] and an additional dimer component appears at high [K^+]. The CD spectra show both 265 nm and 295 nm CD bands of bcl2mid in 5 mM K^+ solution and a strong CD band at 265 nm together with a weak CD band at 295 nm in 150 mM K^+ solution (33). This demonstrates that the major G4 structure of the bcl2mid monomer is the non-parallel form and the major G4 structure of the bcl2mid dimer is the parallel form. Structural conversion, from the monomer to the dimer, depends upon the annealing temperature, with respect to the melting temperature, which increases as a function of K^+ concentration. The high complexity of various G4 structures, under different solution conditions, makes structural analysis even more difficult. Development of a new method for separating the various species present in solution, for further individual study, is of critical importance to the G4 research community.

Previously reported small molecule, 3,6-Bis(1-methyl-4-vinylpyridinium) carbazole diiodide (BMVC) is not only a G4 stabilizer (34), but also a fluorescence probe with higher binding affinity to quadruplex than to duplex DNA (35). Taking these advantageous properties of BMVC into account, a new molecule 3,6-Bis(1-methyl-4-vinylpyridinium)-9-(12′-bromododecyl) carbazole (BMVC-12C-Br) was synthesized by substituting a dodecyl chain at 9-position of BMVC. Due to the hydrophobic moiety of the alkyl chain, this derivative acts as a surfactant between oil and water. After ultrasonic emulsification, an oil-in-water (o/w) emulsion is formed (36). The larger size of the ~2 μm of BMVC-12C-Br emulsion than the 0.22 μm pore size of mixed cellulose esters (MCEs) membrane, together with the binding preference of BMVC-12C-Br emulsion for parallel G4 structures as different from non-parallel G4 structures and DNA duplexes, allows us to demonstrate, for the first time, that the emulsified BMVC-12C-Br can be used to separate different DNA structures after filtration (37). Table 1 lists the DNA sequences studied in this work.

EXPERIMENTAL

Synthesis of BMVC-12C-Br molecule

Synthesis of the BMVC-12C-Br molecule is briefly described in Scheme 1. One gram of 3,6-dibromocarbazole (**1**, ACROS Co.) coupled with 1.5 g 1,12-dibromododecane (ACROS Co.) in the presence of 0.15 g sodium hydride gave excellent yields (92–98%) of 9-alkylcarbazoles (38). The reactions occurred at room temperature for 12 h in THF. The product, 3,6-dibromo-9-(12′-bromododecyl) carbazole (**2**), was extracted using ethyl acetate and recrystallized using methanol. According to the Heck reaction (39), 1 g compound **2** can couple with 4-vinylpyridine

Table 1. The DNA sequences studied in this work

DNA name	Sequence	DNA name	Sequence
HT24	$(T_2AG_3)_4$	LD16	ATGCGCAATTGCGCAT
HT22	$AG_3(T_2AG_3)_3$	T3	$G_3(TG_3)_3$
HT12	$TAG_3T_2AG_3T$	Bcl2mid	$G_3CGCG_3AGGAAG_5CG_3$
Tel24-M	$T_2G_3(T_2AG_3)_3A$	Bcl2mid-M	$G_3CGCG_3AGGAA\underline{TT}G_3CG_3$
Tel19-M	$(TAG_3)_2TG_3TAG_3$	Myc-2345	$TGAG_3TG_4AG_3TG_4AA$
Pu24myc	$TGAG_3TG_4AG_3TG_4A_2G_2$	TBA15	$G_2T_2G_2TGTG_2T_2G_2$

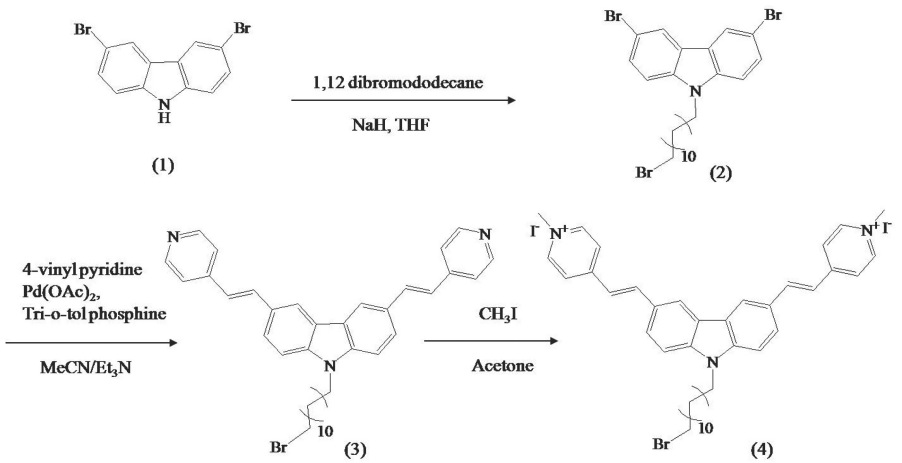

Scheme 1. Synthesis of the BMVC-12C-Br molecule.

(0.8 g, Merck) and mixed powders of Palladium (II) acetate (5 mg, Strem) and tri-*o*-tolyl phosphine (50 mg, Aldrich) under the triethylamine (3 ml)/tetrahydrofuran (9 ml) solvent pairs in a high pressure bottle at 105°C for 48 h. The fluorescent compound 3,6-bis(4-vinylpyridinium)-9-(12′-bromododecyl) carbazole (**3**) was collected and recrystallized using n-hexane with a 20% yield. After refluxing compound **3** with excess CH_3I in Acetone/DMF for 12 h, the orange powder, 3,6-Bis(1-methyl-4-vinylpyridinium)-9-(12′-bromododecyl) carbazole diiodide (**4**) (BMVC-12C-Br), was collected with a 60% yield after recrystallization twice using methanol.

NMR data

^{1}H NMR (d6-DMSO, 400 MHz): δ 8.82 (*d*, *J* = 6.4 Hz, 4H), 8.63 (s, 2H), 8.22 (*d*, *J* = 16 Hz, 4H), 8.21 (*d*, *J* = 6.8 Hz, 2H), 7.94 (*d*, *J* = 8.8 Hz, 2H), 7.79 (*d*, *J* = 8.8 Hz, 2H), 7.57 (*d*, *J* = 16 Hz, 2H), 4.48 (*t*, *J* = 6.4 Hz, 2H), 4.25 (*s*, 6H), 3.07 (*m*, *J* = 8.4 Hz, 2H), 1.80 (*m*, *J* = 6.4 Hz, 2H), 1.54 (*m*, *J* = 6.4 Hz, 2H), 1.13 (*m*, *J* = 6.4 Hz, 16H).

^{13}C NMR (d6-DMSO, 400 MHz): δ (ppm) 153.59, 145.54, 142.63, 127.78, 127.54, 123.63, 123.35, 121.95, 121.29, 111.39, 56.69, 52.65, 47.45, 43.55, 29.67, 29.62, 29.55, 29.49, 29.31, 29.16, 27.13, 26.46, 21.59.

Chemical and sample preparation

All oligonucleotides were purchased from Bio Basic Inc. and used without further purification. Solutions of 10 mM Tris–HCl (pH 7.5) and 150 mM NaCl (or KCl) mixed with each DNA were heated to 95°C for 10 min, cooled slowly to room temperature and then stored overnight at 4°C before use.

Absorption, fluorescence and circular dichroism

Absorption spectra were obtained using a UV-visible spectrophotometer (HELIOS α, Thermo Fisher Scientific, USA), and fluorescence spectra were recorded on a spectrofluorometer (LS-55, PerkinElmer, USA) using a 2-nm band-pass in a 0.1-cm cell length at room temperature. Ten circular dichroism (CD) spectra were obtained using a J-715 spectropolarimeter (Jasco, UK) and an average was taken. A 2 nm bandwidth, a scan speed of 50 nm/min and a step resolution of 0.2 nm were used. The CD spectra were measured under N_2 over the range of 210–350 nm to ascertain the G4 structures.

PAGE

The PAGE was conducted using 20% polyacrylamide gels. Electrophoresis of the gels was carried out at 250 V/cm for 4 h at 4°C. After photography with UV shadowing, the gels were post-stained using 20 μM of BMVC for 30 s at room temperature, and then rinsed with distilled water. They were then photographed under UV light at 254 nm using a digital camera. The fluorescence images of the gels were recorded in a FluoChem HD2 (Alpha Innotech, USA). The relative quantities of the major components in each lane were then measured using an Alphaview program.

CARS and fluorescence microscopic images

The optical setup for CARS microscopy can be found elsewhere (40). Two Ti-sapphire lasers were used to generate CARS and 2PE fluorescence signals simultaneously. A 2.5 ps pulsed laser with a wavelength of 706 nm served as the pump/probe beam for CARS, while a 200 fs pulsed laser with a wavelength of 883.5 nm served as the Stokes beam for CARS and 2PE. The forward CARS scattering signal of the lipid C–H stretching mode at $\sim$2845 cm^{-1} was collected at $\sim$588 nm. The 2PE fluorescence signal from BMVC moieties was collected by epi-detection.

Imino proton NMR

Experiments were performed using 800 MHz Bruker spectrometers at 25°C. 1D NMR spectra were measured in H_2O/D_2O (90%/10%) using a jump and return sequence for solvent suppression. Strand concentration was 0.1 mM; the solution contained 10 mM Tris–HCl (pH 7.5) with a suitable salt condition, external with reference DSS (41).

Analytical ultracentrifugation

Sedimentation experiments were performed using a Beckman Optima XLA analytical ultracentrifuge. Sedimentation velocity experiments of 0.5 OD DNA at 260 nm were conducted at 20°C using a rotor speed of 60 000 rpm. Data analysis was carried out with the program Sedfit (42).

RESULTS AND DISCUSSION

Fluorescence quantum yield and binding affinity

We first investigated if the BMVC-12C-Br molecule maintains its fluorescence and then determined its binding preference to different DNA. Figure 1a shows the absorption and fluorescence spectra of free BMVC-12C-Br and its complexes with DNA of LD16, HT24, T3 and bcl2mid. The molar ratio of BMVC-12C-Br to each DNA structure is 1:1 with a concentration of 20 μM. The absorption band showed red shift upon interaction with DNA. The molar absorption coefficient was decreased by 10–15% for LD16 and HT24 and 30–35% for bcl2mid and T3.

The fluorescence of the free BMVC-12C-Br was quite weak, but the fluorescence increased by at least one order of magnitude upon interaction with these DNA. The fluorescence quantum yield of BMVC-12C-Br is DNA dependent. It was $\sim$0.38 for LD16, $\sim$0.3 for HT24, $\sim$0.12 for T3 and $\sim$0.16 for bcl2mid. These different fluorescence yields for BMVC-12C-Br are probably due to the different binding interactions with the various DNA. Such fluorescence enhancements have been previously observed for BMVC (34).

Figure 1b shows the gel competition assays for the evaluation of the binding preferences of BMVC-12C-Br

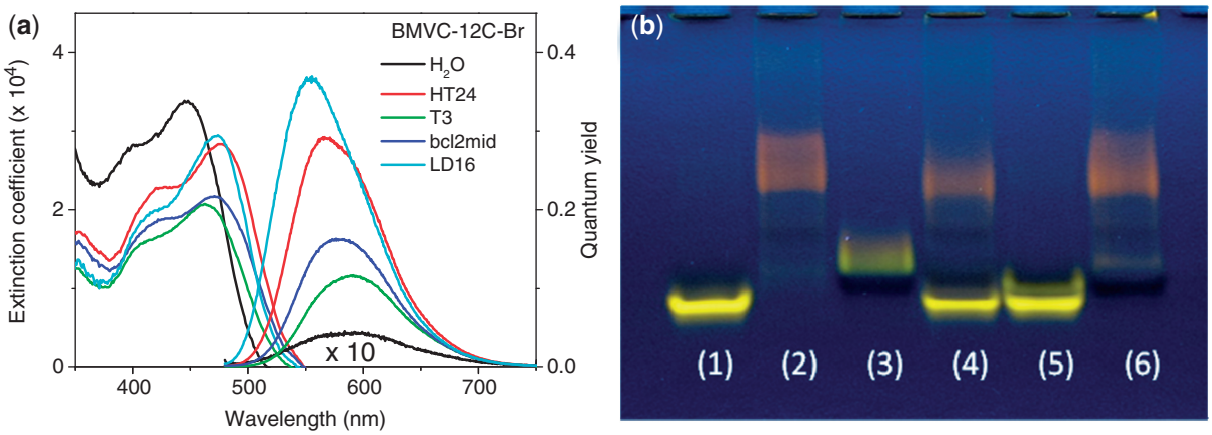

Figure 1. (**a**) The absorption and fluorescence spectra of BMVC-12C-Br molecule and its complexes with various DNAs. (**b**) Gel assays of each 0.2 nmol HT24 (Lane 1), T3 (Lane 2), LD16 (Lane 3), the mixtures of HT24 and T3 (Lane 4), HT24 and LD16 (Lane 5) and T3 and LD16 (Lane 6) incubated with 0.2 nmol BMVC-12C-Br.

to LD16, HT24 and T3. Without competition, visualization of fluorescence from these BMVC-12C-Br bound DNA indicates that BMVC-12C-Br can bind to these DNA. Since the fluorescence was not detected in LD16 in the competition assays, it is suggested that the BMVC-12C-Br has a binding preference for HT24 and T3 over LD16. It is interesting to note that the BMVC-12C-Br bound HT24 complex migrated faster than the free HT24, whereas the BMVC-12C-Br bound T3 complex migrated slower than the free T3. Together with their distinct emissions, these results suggest that BMVC-12C-Br has different binding sites in HT24 and T3 DNA.

Further fluorescence titration was carried out to measure the binding affinities of BMVC-12C-Br to LD16, T3 and HT24. Figure 2 shows the fluorescence spectra of 10 μM of BMVC-12C-Br by adding DNA from 0.25 μM to 8 μM. The fluorescence intensity used to construct the binding plots of γ versus C_f is shown in the inset. The binding ratio γ is defined as C_b/C_{DNA}, where C_f, C_b and C_{DNA} are the molar concentrations of free ligand, bound ligand and DNA, respectively. The difference between C_t and C_b gives the magnitude of C_f, where C_t is the total concentration of ligand. Binding parameters can be obtained by fitting the plots with using a multiple-equivalent-site model (43):

$$\gamma = n\mathrm{K}C_f/(1+\mathrm{K}C_f),$$

where K is the equilibrium binding constant, and n represents the average number of ligands bound per each DNA structure. Note that this equation is identical to the Scatchard equation, $\gamma/C_f = \mathrm{K}(n-\gamma)$. Using the binding plots of γ versus C_f, the problem of obtaining K and n values from slightly nonlinear Scatchard plots becomes irrelevant (44). Here, the binding parameters are measured to be $\mathrm{K} \sim 4.01 \times 10^6$ with $n \sim 4$ to LD16, $\mathrm{K} \sim 2.23 \times 10^7$ with $n \sim 1.9$ to T3, and $\mathrm{K} \sim 1.42 \times 10^7$ with $n \sim 3.1$ to HT24. These results suggest no positive correlation between the fluorescence quantum yield and the binding affinity of BMVC-12C-Br to these DNA.

Emulsification

Since BMVC can be regarded as a hydrophilic site and a 12-carbon chain can act as a hydrophobic site, BMVC-12C-Br can form an oil-in-water (o/w) emulsion by ultrasonic emulsification (36). The emulsification of BMVC-12C-Br was achieved by adding a 0.1 ml squalane (ACROS Co.) to a 0.9 ml of 1 mM BMVC-12C-Br water solution. The mixed solution was subjected to ultrasound for 15 min using an ultrasonic wave with frequency (46 kHz) and power (50 W). The turbid solution was stored in the dark for 2 weeks. The formation of BMVC-12C-Br emulsion was confirmed by coherent anti-Stokes Raman scattering (CARS) and two-photon excitation (2PE) fluorescence microscopy. The overlap of CARS and two-photon fluorescence signals indicates the formation of o/w phase emulsion particles, as shown in Figure 3 (a and b). Here CARS (forward) and two-photon fluorescence (epi) signals were collected simultaneously. The CARS signal at 2845 cm^{-1} is mainly due to the C–H vibrational mode of the squalane located in the center of the emulsion particles. The two-photon excited fluorescence signals from BMVC-12C-Br are mostly distributed on the surface of the emulsion particles.

By changing the polarization of the laser pulses, the brightest fluorescence pattern was always aligned with the laser polarization, as shown in Figure 3 (c and d), mainly due to the parallel alignment of the BMVC-12C-Br dipole and the laser polarization. The distinct fluorescence pattern of the BMVC-12C-Br emulsion suggests that the BMVC moieties are arranged in an orderly fashion on the surface of emulsion particles (45,46).

Separation of G-quadruplex from linear duplex

In order to investigate whether this emulsion could separate HT24 from LD16, we first mixed 20 μM BMVC-12C-Br emulsion with 20 μM each of HT24 and LD16 in 150 mM Na^+ solution for 5 min and then collected the filtrate through a MCE membrane (0.22 μm pore size, Millipore). After filtration, the emulsion was

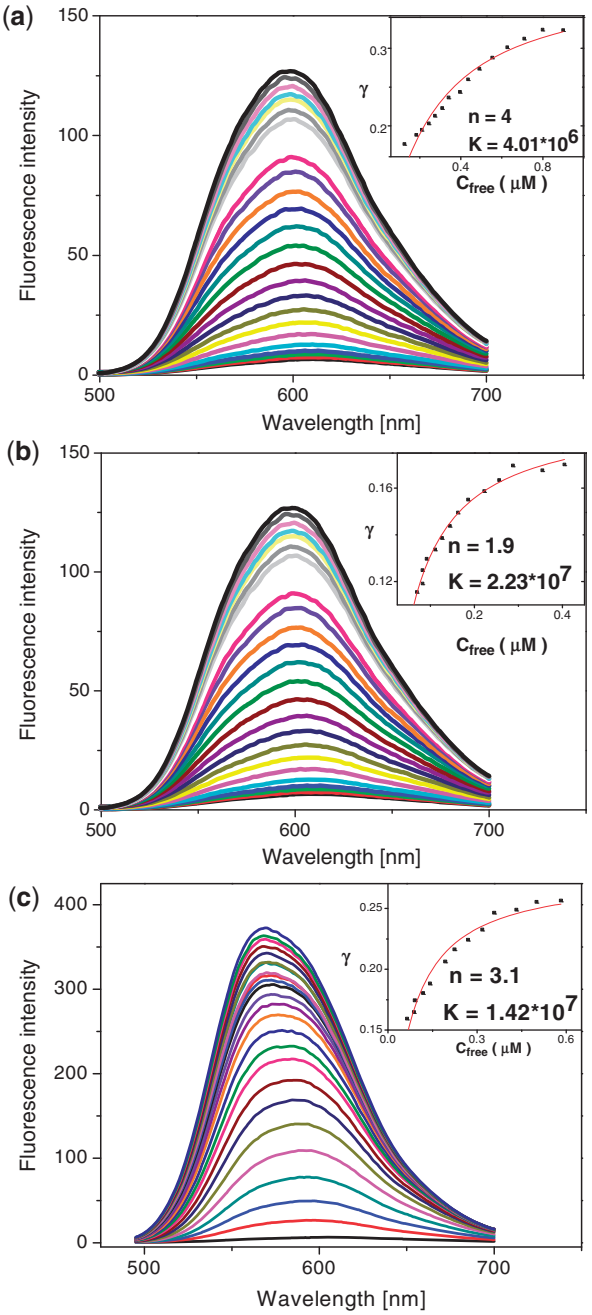

Figure 2. Fluorescence titration of 10 μM BMVC-12C-Br by adding LD (**a**), T3 (**b**), and HT24 (**c**) from 0.25 to 8 μM in Na^+ solution.

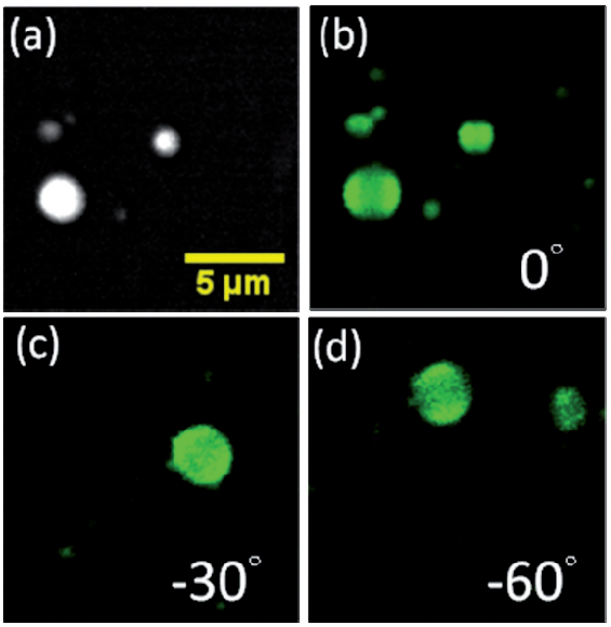

Figure 3. The microscopic images of CARS signals at 2845 cm^{-1} C–H vibrational mode of the squalane inside the emulsion particles (**a**) and 2PE fluorescence signals from BMVC-12C-Br mainly on the surface of the emulsion particles (**b–d**). The images (**a**) and (**b**) were collected simultaneously.

characterized by the presence of fluorescence on the membrane while the filtrate was clear and transparent.

Figure 4a shows the CD spectra before and after six sequences of emulsion-induced filtration (EIF). A discernible decrease in the 295 nm CD signal was detected after each EIF. This change was not observed in the filtrate from the HT24/LD16 mixture without emulsion. Figure 4b shows the spectral difference between the CD spectra before filtration and after the final EIF. The CD pattern for the spectral difference is quite similar to the CD pattern for HT24, implying the loss of the HT24 component after EIF. In addition, the CD pattern observed after the final EIF is very similar to the CD pattern for LD16, as shown in Figure 4b. It appears that the BMVC-12C-Br emulsion has a high-binding preference for G-quadruplex HT24 over duplex LD16.

We further investigated whether BMVC-12C-Br emulsion could be used to separate different G4 structures. Figure 4c shows the CD spectra for equal amounts of two well characterized G4 structures; an antiparallel basket G4 structure of HT24 (28) and a parallel propeller G4 structure of ($G_3TG_3TG_3TG_3$) (T3) (47), mixed in 150 mM Na^+ solution before and after two sequences of EIF. The spectral difference between the final and initial spectra is almost identical to the CD spectrum of T3, as shown in the inset of Figure 4c. It appears that BMVC-12C-Br emulsion has better binding ability to the parallel G4 structure of T3 than the antiparallel G4 structure of HT24.

Gel assays were performed on the HT24/T3 mixture before and after two sequences of EIF and staining by BMVC. The stained gels were put into a FluoChem HD2 and the fluorescence images were recorded, as shown in Figure 4d. Since the fluorescence yield of BMVC is DNA dependent (34), different staining efficiencies are evident for HT24 and T3 in Figure 4d. Nevertheless, the intensity change for each DNA after each EIF can be estimated independently. The results show a large decrease in the T3 component, but only a slight change in the HT24 component after EIF. Analysis of the 73% loss and 27% loss of the 265 nm CD band shows good correlation with the 68% loss and 29% loss of the T3 component in the gel assays after the first and the second sequences of EIF, respectively.

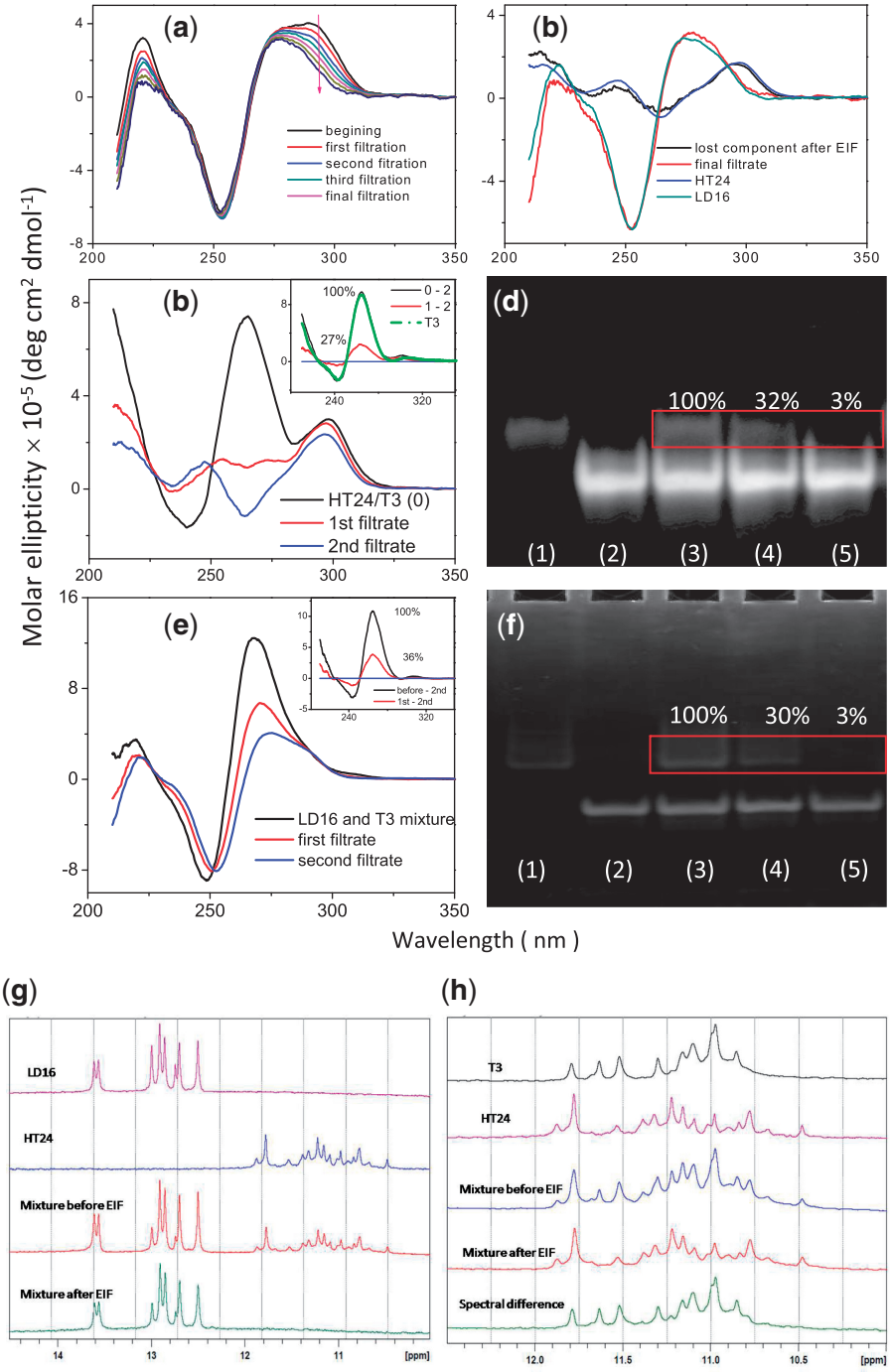

Figure 4. (**a**) CD spectra of 20 μM HT24 and 20 μM LD16 mixture in 150 mM Na^+ solution before and after six sequences of EIF. (**b**) Comparison of the spectral difference between the initial and the final spectra (black) with the CD spectrum of HT24 in 150 mM Na^+ solution (blue). Also comparison of the final filtrate (red) and LD16 (green) in 150 mM Na^+. (**c**) CD spectra of 20 μM HT24 and 20 μM T3 mixture before and after two sequences of EIF. The inset shows the spectral difference between each spectrum and the final spectrum (solid line), and the CD spectrum of T3 (green dash line). (**d**) Gel assays of T3 (Lane 1), HT24 (Lane 2) and the mixture of them before (Lane 3), and after two sequences of EIF (Lanes 4 and 5) stained by BMVC for 30 s. (**e**) CD spectra of 20 μM LD16 and 20 μM T3 mixture before and after two sequences of EIF. The inset shows the spectral difference between each spectrum and the final spectrum. (**f**) Gel assays of T3 (Lane 1), LD16 (Lane 2) and the mixture of them before (Lane 3) and after two sequences of EIF (Lanes 4 and 5) stained by BMVC for 30 s. (**g** and **h**) NMR spectra of DNA sequences of LD16, HT24 and T3 before and after EIF.

Note that the CD spectra of HT24, shown in Figure 4b (blue) and Figure 4c (blue), are very similar to each other, indicating that BMVC-12C-Br emulsion can effectively bind to the parallel G4 structure of T3 and therefore isolate the antiparallel G4 structure of HT24 from the conformational mixture. To our knowledge, this is the first demonstration of the isolation of specific G4 structure.

Figure 4e shows the CD spectra for 20 μM each of T3 and LD16 in 150 mM Na^+ solution before and after two sequences of EIF. The results show a large decrease in the T3 component, but no appreciable change in the LD16 component after EIF. The gel assays (Figure 4f) further confirm this finding. Compared to the separation of the linear duplex of LD16 from the anti-parallel G4 structure of HT24, it appears that BMVC-12C-Br emulsion is more efficient in separating the LD16 from the parallel G4 structure of T3 after filtration.

We further performed imino proton NMR to examine whether the NMR spectra of these DNA structures can be separated after EIF. Figure 4g shows the imino proton NMR spectra of 100 μM LD16, 100 μM HT24 and the mixture of them before and after EIF in 150 mM Na^+ solution. It is found that the imino protons are located at 10.5-12.5 ppm for G4 structure and at 12.5–14 ppm for Watson–Crick duplex (48). The spectrum for the mixture after EIF is almost identical to the spectrum of LD16, indicating that BMVC-12C-Br EIF is able to separate LD16 linear duplex from HT24 G4 structure.

Figure 4h shows the NMR spectra for 100 μM HT24, 100 μM T3 and the mixture of them before and after EIF in 150 mM Na^+ solution together with the spectral difference for the mixture before and after EIF. The NMR spectrum for the mixture after EIF is quite similar to the spectrum for HT24. In addition, the spectral difference for the mixture before and after EIF is very similar to the spectrum for T3. It appears that BMVC-12C-Br EIF is also good for the separation of anti-parallel from parallel G4 structures. Moreover, it is possible to obtain an individual spectrum of one for DNA in the filtrate and one for DNA bound by emulsion for further structural analyses.

Separation of parallel from non-parallel G-quadruplexes

Although the precise structures of HT22 in K^+ solution remain undetermined, the structures of two modified telomeric sequences, Tel24-M (49) and Tel19-M (50) were analyzed by NMR. Patel *et al.* (49) have shown that the hybrid type antiparallel G4 structure is the major conformation of Tel24-M in K^+ solution, while Phan *et al.* [50] have illustrated that the propeller type parallel G4 structure is predominant conformation of Tel19-M in K^+ solution. Figure 5a shows the NMR spectra for 100 μM Tel24-M, 100 μM Tel19-M and the mixture of them before and after EIF in 150 mM K^+ solution together with the spectral difference before and after EIF. Both NMR spectra are very consistent with the documented spectra (49,50). Of importance is that the spectrum for the mixture after EIF is almost identical to the spectrum of Tel24-M and the spectral difference for the mixture before and after EIF is the same as the spectrum of Tel19-M. The gel assays (Figure 5b) further confirm this finding, i.e. a large decrease in the Tel19-M component, but a slight decrease in the Tel24-M component after EIF. It is suggested that BMVC-12C-Br EIF is able to separate Tel24-M hybrid type from Tel19-M propeller type G4 structures.

Another pair of G-rich sequences from gene promoter regions is used to further illustrate this EIF method. NMR analyses showed that a hybrid type G4 structure is the major conformation for a sequence of bcl2mid-M (32) and a parallel type G4 structure is predominated for a sequence of Myc-2345 (51) in K^+ solution. Figure 5c shows the NMR spectra for 100 μM bcl2mid-M, 100 μM Myc-2345 and the mixture of them before and after EIF in 150 mM K^+ solution together with the spectral difference before and after EIF. Both NMR spectra are very consistent with the documented spectra (32,51). Again, the spectrum after EIF is almost identical to the spectrum for bcl2mid-M and the spectral difference before and after EIF is the same as the spectrum for Myc-2345. The gel assays (Figure 5d) also show a large decrease in the Myc-2345 component, but only a slight change in the bcl2mid-M component after EIF. Similar NMR and gel results were also observed for the separation of TBA antiparallel G4 structure from Pu24myc parallel G4 structure in K^+ solution after EIF (data not shown). These results clearly indicate that this EIF method can well separate the non-parallel G4 structures from the parallel G4 structures.

In addition, NMR analysis shows that the two repeated human telomeric sequence HT12 can form both parallel and anti-parallel G4 structures in K^+ solution (48). Figure 5e shows the CD spectra of HT12 in 150 mM K^+ solution before and after two sequences of EIF. The large decrease in the 265 nm CD band after the first filtration suggests that parallel G4 structures can be separated after EIF, as shown in the inset. Moreover, Figure 5f shows the imino proton NMR of HT12 in 150 mM K^+ solution before and after EIF together with the spectral difference between them. There are a set of minor peaks and a set of major peaks in the spectrum before EIF, which are consistent with the previous NMR analysis (48). After EIF, the minor peaks remained in the filtrate are due to anti-parallel G4 structure and the major peaks obtained from the spectral difference are attributed to parallel G4 structure. It is suggested that BMVC-12C-Br emulsion can separate the antiparallel type from the parallel type G4 structures formed by the same G-rich sequence.

The parallel G4 structures of HT22 in K^+ solution?

We now are able to verify whether the parallel G4 structure is a major conformation of HT22 in 150 mM K^+ solution. The absence of a large change in the 265 nm CD band and no appreciable difference in the imino proton NMR spectra after EIF (data not shown) suggest that the parallel G4 structure is not a major conformation of HT22 in K^+ solution.

It is found that the human telomere can adopt a parallel G4 structure in K^+ solution under molecular crowding conditions by the addition of 40% (w/v) PEG 200 (31,52). Recently, a number of studies showed that PEG acts as a dehydrating agent than as a crowding agent (53,54). It is of interest to investigate whether BMVC-12C-Br emulsion can separate the parallel form after structural conversion from the non-parallel form under PEG condition. Figure 6a shows the CD spectra of

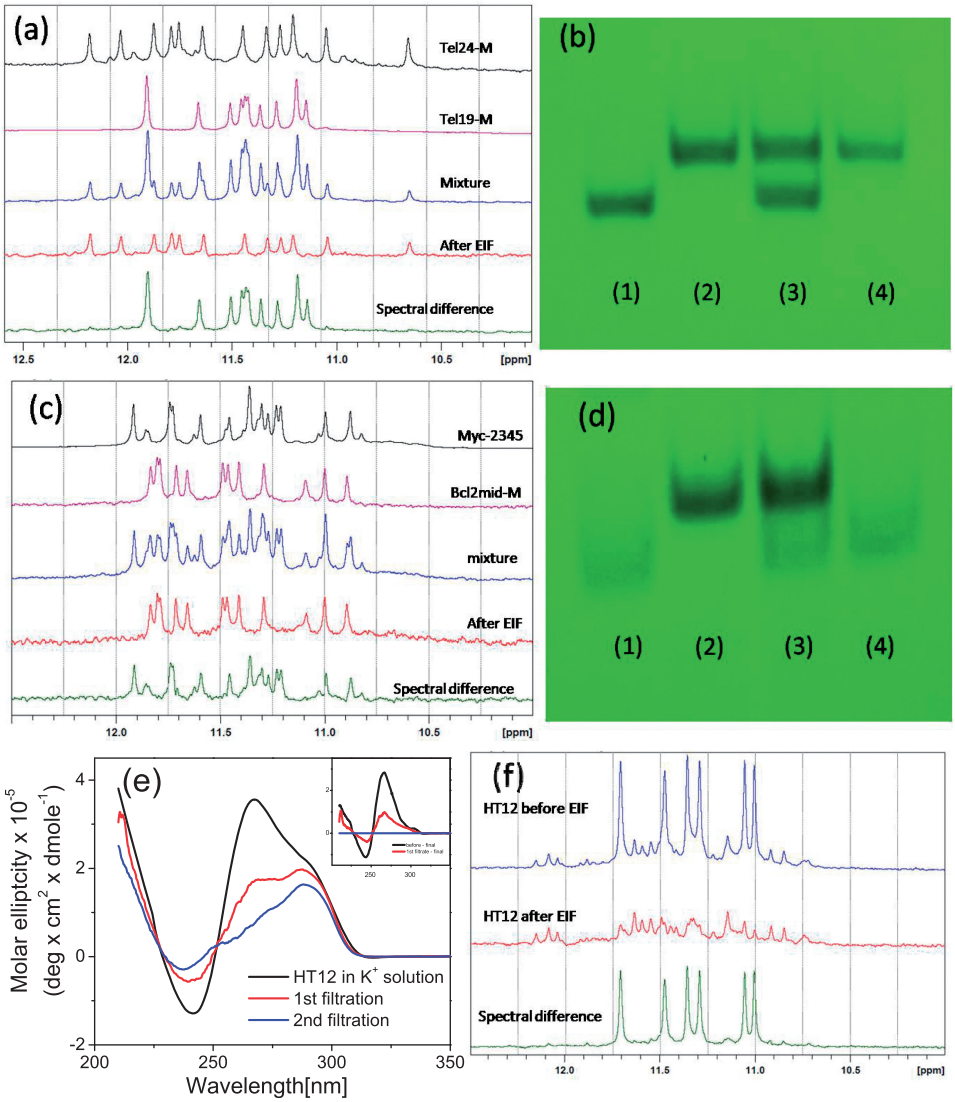

Figure 5. (**a**) NMR spectra of Tel24-M and Tel19-M in 150 mM K^+ solution before and after EIF. (**b**) Gel assays of Tel19-M (Lane 1), Tel24-M (Lane 2) and the mixture of them before (Lane 3) and after EIF (Lane 4). (**c**) NMR spectra of bcl2mid-M and Myc2345 in 150 mM K^+ solution before and after EIF. (**d**) Gel assays of bcl2mid-M (Lane 1), Myc-2345 (Lane 2), the mixture of them before (Lane 3) and after EIF (Lane 4). (**e**) CD and (**f**) NMR spectra of HT12 in 150 mM K^+ solution before and after EIF.

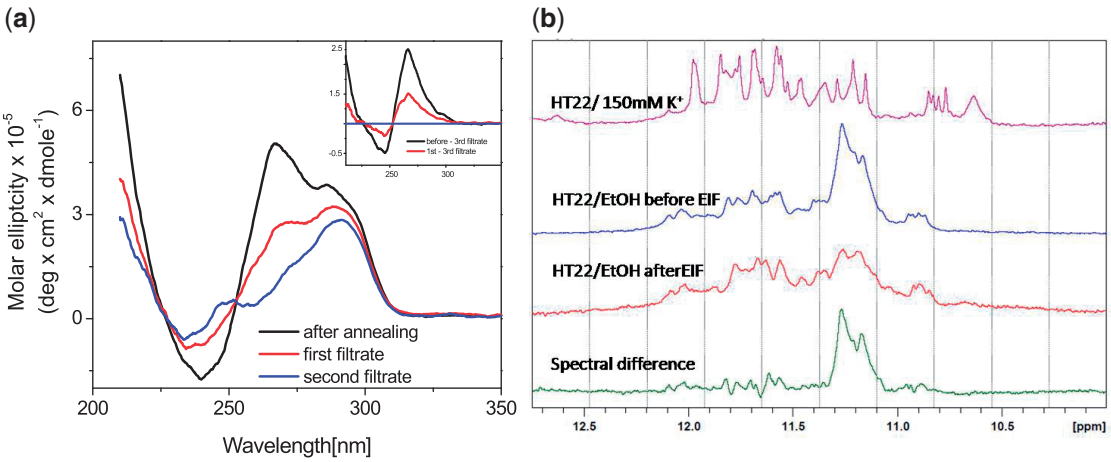

Figure 6. (**a**) CD spectra of HT22 in 150 mM K^+ solution upon addition of 40% (w/v) PEG 200 before and after two sequences of EIF. The inset shows spectral difference between each spectrum and the final spectrum. (**b**) NMR spectra of HT22 and upon addition of 50% (v/v) EtOH for overnight before and after EIF together with their spectral difference.

HT22 in 150 mM K^+ solution and upon adding 40% (w/v) PEG 200 before and after two sequences of EIF. After addition of the PEG 200, the appreciable increase in the 265 nm CD band together with the decrease in the 295 nm CD band indicates a structural change in HT22. Again, the significant decrease in the 265 nm CD band after each EIF is consistent with the previous results, i.e. the parallel G4 structure after conversion is selected by the BMVC-12C-Br emulsion. It further verifies the structural change from the non-parallel type G4 structure to the parallel G4 structure of HT22 when a dehydrating agent exists.

Since PEG is inconvenient for NMR spectrum and has a high viscosity and a low dielectric constant, Trent *et al.* (53) used acetonitrile as a dehydrating agent and found similar conformational transitions of HT22 in K^+ solution. Here, we use ethanol as a dehydrating agent (55) because the acetonitrile can damage MCE membrane. Figure 6b shows the imino proton NMR spectra of HT22 in 150 mM K^+ solution and upon addition of 50% (v/v) ethanol for overnight before and after EIF together with the spectral difference between them. The NMR spectra of HT22 in K^+ solution show significant changes after addition of ethanol. Considering that BMVC-12C-Br emulsion has better selectivity to the parallel structure, it is likely that the spectral difference characterized by the major signals between 11.1 and 11.3 ppm is due to the parallel type G4 structure. Further study of this difference spectrum may be useful in determining the precise structure of the converted conformation of HT22.

High order G4 structures

We now examine whether BMVC-12C-Br emulsion can be used to separate bcl2mid monomer from the bcl2mid dimer formed in 150 mM K^+ solution. Figure 7a shows the gel assays of bcl2mid before and after two sequences of EIF. We found a dramatic decrease in the dimer components, but a slight decrease in the monomer component after EIF. Again, Figure 7b shows a significant decrease in the 265 nm CD band after EIF. The 64% loss and 33% loss of the dimer component in the gel assays correlates well with the 67% decrease and 33% decrease in the 265 nm CD band after two sequences of EIF, indicating

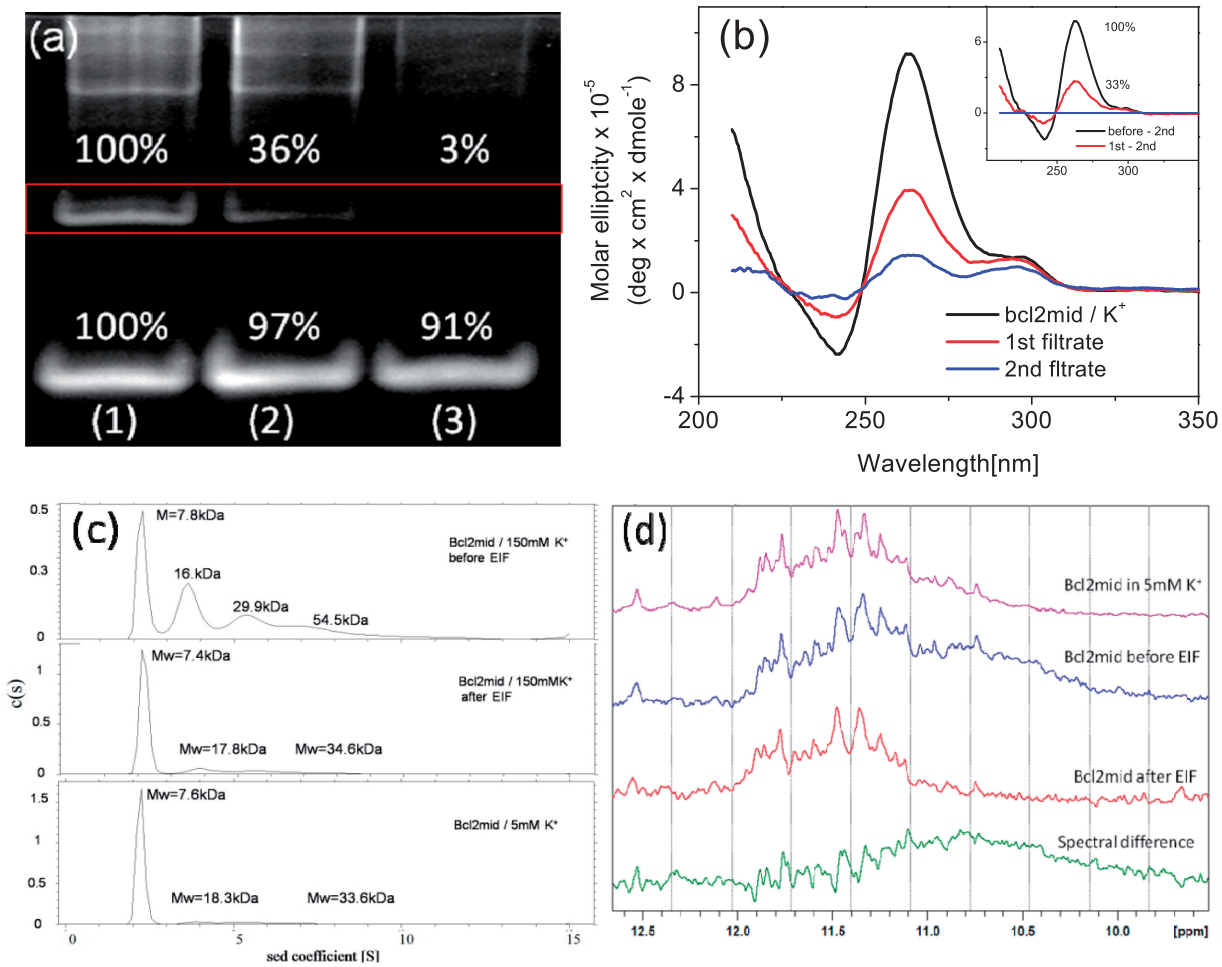

Figure 7. (**a**) Gel assays of bcl2mid before (Lane 1) and after two sequences of filtration (Lanes 2 and 3). (**b**) CD spectra of bcl2mid in 150 mM K^+ solution before and after two sequences of EIF. The inset shows spectral difference between each spectrum and the final spectrum. (**c**) Ultra centrifugation of bcl2mid in 150 mM K^+ solution before and after EIF and bcl2mid in 5 mM K^+ solution. (**d**) NMR spectra of Bcl2mid in 5 mM K^+ solution and in 150 mM K^+ solution before and after EIF together with their spectral difference.

that BMVC-12C-Br emulsion has better selectivity to dimer than monomer of bcl2mid.

Furthermore, sedimentation methods based on ultracentrifugation analysis (56,57) are used for the characterization of monomer, dimer and high-order structures of bcl2mid. Figure 7c show the sedimentation results of bcl2mid in 5 mM K^+ solution and bcl2mid in 150 mM K^+ solution before and after EIF. Since molecular weight of each species can be measured directly by experiment, a major component of bcl2mid monomer is detected in 5 mM K^+ solution, while multiple species including monomer, dimer and tetramer are found in 150 mM K^+ solution, which are consistent with the findings in gel assays. After EIF, significant decrease of the intermolecular species indicates that BMVC-12C-Br emulsion selects intermolecular species of bcl2mid and the complexes are trapped in the membrane. In contrast, no appreciable difference of the monomer suggests that the intramolecular species free from emulsion are isolated in the filtrate.

Figure 7d shows the imino proton NMR spectra of 100 μM bcl2mid in 150 mM K^+ solution before and after EIF together with the spectral difference between them. The spectra presented, the imino region for quadruplex DNA, are typical of a mixture of several conformations. Since BMVC-12C-Br EIF can separate intramolecular from intermolecular G4 structures, a broad envelope with some fine lines at 11–12 ppm in the NMR spectrum after EIF suggests that at least two different G4 structures of bcl2mid monomer coexist in a K^+ solution. In addition, a weak broad envelope centered at ~10.8 ppm in the difference spectrum is mainly due to multiple intermolecular species of bcl2mid. This weak broad envelope in the difference spectrum is further confirmed by using 400 μM bcl2mid in 150 mM K^+ solution before and after EIF (data not shown).

To further compare the bcl2mid monomer obtained directly from the predominant component of bcl2mid in 5 mM K^+ solution (33) and indirectly from the filtrate of bcl2mid in 150 mM K^+ solution, Figure 7d also shows an NMR spectrum of bcl2mid monomer prepared in 5 mM K^+ solution annealed at 95°C and then augmented with potassium to 150 mM, which is very similar to the documented spectrum (41). Although CD cannot give precise structures of these G-quadruplexes, it can be used to distinguish parallel and antiparallel G4 structures based on their strand orientation (58). The absence of the 295 nm CD signal in the difference spectrum suggests that the parallel type G4 structures are predominated in the intermolecular conformers of bcl2mid. Such parallel type G4 structure was found in the Pu22myc dimer (59). In addition, this EIF method can isolate the non-parallel type G4 structures in the filtrate from the parallel type G4 structures in the membrane. The broad envelope shown in the NMR spectrum after EIF suggests that at least two non-parallel G4 structures coexist in bcl2mid monomer. Similarly, the broad envelope shown in the difference spectrum also suggests that multiple parallel G4 structures co-exist in the intermolecular species of bcl2mid. Thus, the coexistence of the multiple conformers causes the problem for determining the structure of each conformer of bcl2mid.

In summary, we have demonstrated a novel method for the structural separation of G-quadruplex DNA. This method combines a methodology for membrane emulsion/filtration and a lipophilic analogue of BMVC that can form an oil-in-water emulsion with high binding affinity to specific DNA structure. The BMVC-12C-Br EIF process has been proven to separate linear duplexes from G4 structures and non-parallel G4 structures from parallel G4 structures. The spectrum obtained after EIF treatment is mainly determined by the DNA in the filtrate and the spectrum obtained from the difference before and after EIF treatment can be attributed to the DNA bound by the emulsion. This process provides information useful in establishing spectrum–structure correlation. The process can also be used to identify parallel and non-parallel G4 structures for unknown G-rich sequences. These data provide 'proof-of-concept' evidence for the selective targeting of emulsified agents to specific DNA structure for structural separation. The general process could have a significant impact on this field and others.

ACKNOWLEDGEMENTS

The authors would like to thank Dr Shing-Jong Huang (Instrumentation Center, National Taiwan University) for assistance in obtaining the Bruker AVIII 800 MHz FT-NMR data. We thank Mr Yusen Wu and Dr Shu-Chuan Jao (Biophysics Core Facility in Institute of Biological Chemistry, Academia Sinica) for kindly providing the sedimentation measurements.

FUNDING

Funding for open access charge: Academia Sinica (AS-98-TP-A04); National Science Council of the Republic of China (Grant NSC-98-2113-M001-025).

Conflict of interest statement. None declared.

REFERENCES

1. Huppert,J.L. and Balasubramanian,S. (2007) G-quadruplexes in promoters throughout the human genome. *Nucleic Acids Res.*, **35**, 406–413.
2. Todd,A.K., Haider,S.M., Parkinson,G.N. and Neidle,S. (2007) Sequence occurrence and structural uniqueness of a G-quadruplex in the human c-kit promoter. *Nucleic Acids Res.*, **35**, 5799–5808.
3. Qin,Y. and Hurley,L.H. (2008) Structures, folding patterns, and functions of intramolecular DNA G-quadruplexes found in eukaryotic promoter regions. *Biochimie*, **90**, 1149–1171.
4. Hurley,L.H. (2002) DNA and its associated processes as targets for cancer therapy. *Nat. Rev. Cancer*, **2**, 188–200.
5. Rezler,E.M., Bearss,D.J. and Hurley,L.H. (2003) Telomere inhibition and telomere disruption as processes for drug targeting. *Annu. Rev. Pharmacol. Toxicol.*, **43**, 359–379.
6. Mikami-Terao,Y., Akiyama,M., Yuza,Y., Yanagisawa,T., Yamada,O. and Yamada,H. (2008) Antitumor activity of G-quadruplex-interactive agent TMPyP4 in K562 leukemic cells. *Cancer Lett.*, **261**, 226–234.
7. Balasubramanian,S. and Neidle,S. (2009) G-quadruplex nucleic acids as therapeutic targets. *Curr. Opin. Chem. Biol.*, **13**, 345–353.

8. Neidle,S. (2010) Human telomeric G-quadruplex: the current status of telomeric G-quadruplexes as therapeutic targets in human cancer. *FEBS J.*, **277**, 1118–1125.
9. Autexier,C. and Greider,C.W. (1996) Telomerase and cancer: revisiting the telomere hypothesis. *Trends Biochem. Sci.*, **21**, 387–391.
10. Zahler,A.M., Williamson,J.R., Cech,T.R. and Prescott,D.M. (1991) Inhibition of telomerase by G-quartet DNA structures. *Nature*, **350**, 718–720.
11. Mergny,J.L. and Helene,C. (1998) G-quadruplex DNA: a target for drug design. *Nat. Med.*, **4**, 1366–1367.
12. Neidle,S. and Parkinson,G. (2002) Telomere maintenance as a target for anticancer drug discovery. *Nat. Rev. Drug Discov.*, **1**, 383–393.
13. Oganesian,L. and Bryan,T.M. (2007) Physiological relevance of telomeric G-quadruplex formation: a potential drug target. *Bioessays*, **29**, 155–165.
14. Wong,H.M., Payet,L. and Huppert,J.L. (2009) Function and targeting of G-quadruplexes. *Curr. Opin. Mol. Ther.*, **11**, 146–155.
15. Dexheimer,T.S., Sun,D. and Hurley,L.H. (2006) Deconvoluting the structural and drug-recognition complexity of the G-quadruplex-forming region upstream of the bcl-2 P1 promoter. *J. Am. Chem. Soc.*, **128**, 5404–5415.
16. Akagi,T., Kondo,E. and Yoshino,T. (1994) Expression of Bcl-2 protein and Bcl-2 mRNA in normal and neoplastic lymphoid tissues. *Leuk. Lymphoma*, **13**, 81–87.
17. Joensuu,H., Pylkkanen,L. and Toikkanen,S. (1994) Bcl-2 protein expression and long-term survival in breast cancer. *Am. J. Pathol.*, **145**, 1191–1198.
18. Tjalma,W., De Cuyper,E., Weyler,J., Van Marck,E., De Pooter,C., Albertyn,G. and van Dam,P. (1998) Expression of bcl-2 in invasive and in situ carcinoma of the uterine cervix. *Am. J. Obstet. Gynecol.*, **178**, 113–117.
19. Pezzella,F., Turley,H., Kuzu,I., Tungekar,M.F., Dunnill,M.S., Pierce,C.B., Harris,A., Gatter,K.C. and Mason,D.Y. (1993) bcl-2 protein in non-small-cell lung carcinoma. *N. Engl. J. Med.*, **329**, 690–694.
20. McDonnell,T.J., Troncoso,P., Brisbay,S.M., Logothetis,C., Chung,L.W., Hsieh,J.T., Tu,S.M. and Campbell,M.L. (1992) Expression of the protooncogene bcl-2 in the prostate and its association with emergence of androgen-independent prostate cancer. *Cancer Res.*, **52**, 6940–6944.
21. Baretton,G.B., Diebold,J., Christoforis,G., Vogt,M., Muller,C., Dopfer,K., Schneiderbanger,K., Schmidt,M. and Lohrs,U. (1996) Apoptosis and immunohistochemical bcl-2 expression in colorectal adenomas and carcinomas. Aspects of carcinogenesis and prognostic significance. *Cancer*, **77**, 255–264.
22. Onyshchenko,M.I., Gaynutdinov,T.I., Englund,E.A., Appella,D.H., Neumann,R.D. and Panyutin,I.G. (2009) Stabilization of G-quadruplex in the BCL2 promoter region in double-stranded DNA by invading short PNAs. *Nucleic Acids Res.*, **37**, 7570–7580.
23. Wang,X.D., Ou,T.M., Lu,Y.J., Li,Z., Xu,Z., Xi,C., Tan,J.H., Huang,S.L., An,L.K., Li,D. *et al.* (2010) Turning off transcription of the bcl-2 gene by stabilizing the bcl-2 promoter quadruplex with quindoline derivatives. *J. Med. Chem.*, **53**, 4390–4398.
24. Nambiar,M., Goldsmith,G., Moorthy,B.T., Lieber,M.R., Joshi,M.V., Choudhary,B., Hosur,R.V. and Raghavan,S.C. (2011) Formation of a G-quadruplex at the BCL2 major breakpoint region of the t(14;18) translocation in follicular lymphoma. *Nucleic Acids Res.*, **39**, 936–948.
25. Sundquist,W.I. and Klug,A. (1989) Telomeric DNA dimerizes by formation of guanine tetrads between hairpin loops. *Nature*, **342**, 825–829.
26. Davis,J.T. (2004) G-quartets 40 years later: from 5′-GMP to molecular biology and supramolecular chemistry. *Angew. Chem. Int. Ed. Engl.*, **43**, 668–698.
27. Burge,S., Parkinson,G.N., Hazel,P., Todd,A.K. and Neidle,S. (2006) Quadruplex DNA: sequence, topology and structure. *Nucleic Acids Res.*, **34**, 5402–5415.
28. Wang,Y. and Patel,D.J. (1993) Solution structure of the human telomeric repeat d[AG3(T2AG3)3] G-tetraplex. *Structure*, **1**, 263–282.
29. Parkinson,G.N., Lee,M.P. and Neidle,S. (2002) Crystal structure of parallel quadruplexes from human telomeric DNA. *Nature*, **417**, 876–880.
30. Zhang,Z., Dai,J., Veliath,E., Jones,R.A. and Yang,D. (2010) Structure of a two-G-tetrad intramolecular G-quadruplex formed by a variant human telomeric sequence in K+ solution: insights into the interconversion of human telomeric G-quadruplex structures. *Nucleic Acids Res.*, **38**, 1009–1021.
31. Xue,Y., Kan,Z.Y., Wang,Q., Yao,Y., Liu,J., Hao,Y.H. and Tan,Z. (2007) Human telomeric DNA forms parallel-stranded intramolecular G-quadruplex in K^+ solution under molecular crowding condition. *J. Am. Chem. Soc.*, **129**, 11185–11191.
32. Dai,J., Chen,D., Jones,R.A., Hurley,L.H. and Yang,D. (2006) NMR solution structure of the major G-quadruplex structure formed in the human BCL2 promoter region. *Nucleic Acids Res.*, **34**, 5133–5144.
33. Lin,C.T., Tseng,T.Y., Wang,Z.F. and Chang,T.C. (2011) Structural conversion of intramolecular and intermolecular G-quadruplexes of bcl2mid: the effect of potassium concentration and ion exchange. *J. Phys. Chem. B.*, **115**, 2360–2370.
34. Chang,C.C., Wu,J.Y., Chien,C.W., Wu,W.S., Liu,H., Kang,C.C., Yu,L.J. and Chang,T.C. (2003) A fluorescent carbazole derivative: high sensitivity for quadruplex DNA. *Anal. Chem.*, **75**, 6177–6183.
35. Chang,C.C., Kuo,I.C., Ling,I.F., Chen,C.T., Chen,H.C., Lou,P.J., Lin,J.J. and Chang,T.C. (2004) Detection of quadruplex DNA structures in human telomeres by a fluorescent carbazole derivative. *Anal. Chem.*, **76**, 4490–4494.
36. Sherman,P. (ed.), (1968) *Emulsion Science*. Academic Press, London; New York, p. 43.
37. De Bruin,T.J., Marcelis,A.T., Zuilhof,H., Rodenburg,L.M., Niederlander,H.A., Koudijs,A., Overdevest,P.E., Van der Padt,A. and Sudholter,E.J. (2000) Separation of amino acid enantiomers by micelle-enhanced ultrafiltration. *Chirality*, **12**, 627–636.
38. Manickam,M., Belloni,M., Kumar,S., Varshney,S.K., Shankar Rao,D.S., Ashton,P.R., Preece,J.A. and Spencer,N. (2001) The first hexagonal columnar discotic liquid crystalline carbazole derivatives induced by noncovalent π–π interactions. *J. Mater. Chem.*, **11**, 2790–2800.
39. Chang,T.-C., Chang,C.C. and Wu,J.Y. (2005) *Quadruplex Stabilizer*, US patent No. 6979738 B2.
40. Chien,C.H., Chen,W.W., Wu,J.T. and Chang,T.C. (2011) Label-free imaging of Drosophila in vivo by coherent anti-Stokes Raman scattering and two-photon excitation autofluorescence microscopy. *J. Biomed. Opt.*, **16**, 016012.
41. Dai,J., Dexheimer,T.S., Chen,D., Carver,M., Ambrus,A., Jones,R.A. and Yang,D. (2006) An intramolecular G-quadruplex structure with mixed parallel/antiparallel G-strands formed in the human BCL-2 promoter region in solution. *J. Am. Chem. Soc.*, **128**, 1096–1098.
42. Schuck,P., Perugini,M.A., Gonzales,N.R., Howlett,G.J. and Schubert,D. (2002) Size-distribution analysis of proteins by analytical ultracentrifugation: strategies and application to model systems. *Biophys. J.*, **82**, 1096–1111.
43. Chaires,J.B. (2001) Analysis and interpretation of ligand-DNA binding isotherms. *Methods Enzymol.*, **340**, 3–22.
44. Chang,C.C., Chien,C.W., Lin,Y.H., Kang,C.C. and Chang,T.C. (2007) Investigation of spectral conversion of d(TTAGGG)4 and d(TTAGGG)13 upon potassium titration by a G-quadruplex recognizer BMVC molecule. *Nucleic Acids Res.*, **35**, 2846–2860.
45. Bagatolli,L.A. and Gratton,E. (1999) Two-photon fluorescence microscopy observation of shape changes at the phase transition in phospholipid giant unilamellar vesicles. *Biophys. J.*, **77**, 2090–2101.
46. Le,T.T., Rehrer,C.W., Huff,T.B., Nichols,M.B., Camarillo,I.G. and Cheng,J.X. (2007) Nonlinear optical imaging to evaluate the impact of obesity on mammary gland and tumor stroma. *Mol. Imaging*, **6**, 205–211.
47. Viglasky,V., Bauer,L. and Tluckova,K. (2010) Structural features of intra- and intermolecular G-quadruplexes derived from telomeric repeats. *Biochemistry*, **49**, 2110–2120.
48. Phan,A.T. and Patel,D.J. (2003) Two-repeat human telomeric d(TAGGGTTAGGGT) sequence forms interconverting parallel and antiparallel G-quadruplexes in solution: distinct topologies,

thermodynamic properties, and folding/unfolding kinetics. *J. Am. Chem. Soc.*, **125**, 15021–15027.
49. Luu,K.N., Phan,A.T., Kuryavyi,V., Lacroix,L. and Patel,D.J. (2006) Structure of the human telomere in K+ solution: an intramolecular (3 + 1) G-quadruplex scaffold. *J. Am. Chem. Soc.*, **128**, 9963–9970.
50. Hu,L., Lim,K.W., Bouaziz,S. and Phan,A.T. (2009) Giardia telomeric sequence $d(TAGGG)_4$ forms two intramolecular G-quadruplexes in K+ solution: effect of loop length and sequence on the folding topology. *J. Am. Chem. Soc.*, **131**, 16824–16831.
51. Phan,A.T., Modi,Y.S. and Patel,D.J. (2004) Propeller-type parallel-stranded G-quadruplexes in the human c-myc promoter. *J. Am. Chem. Soc.*, **126**, 8710–8716.
52. Kasuga,T., Townsend,J.P., Tian,C., Gilbert,L.B., Mannhaupt,G., Taylor,J.W. and Glass,N.L. (2005) Long-oligomer microarray profiling in Neurospora crassa reveals the transcriptional program underlying biochemical and physiological events of conidial germination. *Nucleic Acids Res.*, **33**, 6469–6485.
53. Miller,M.C., Buscaglia,R., Chaires,J.B., Lane,A.N. and Trent,J.O. (2010) Hydration is a major determinant of the G-quadruplex stability and conformation of the human telomere 3′ sequence of $d(AG_3(TTAG_3)_3)$. *J. Am. Chem. Soc.*, **132**, 17105–17107.
54. Hansel,R., Lohr,F., Foldynova-Trantirkova,S., Bamberg,E., Trantirek,L. and Dotsch,V. (2011) The parallel G-quadruplex structure of vertebrate telomeric repeat sequences is not the preferred folding topology under physiological conditions. *Nucleic Acids Res.* (30 March 2011, date last accessed) [Epub ahead of print; doi:10.1093/nar/gkr174].
55. Renciuk,D., Kejnovska,I., Skolakova,P., Bednarova,K., Motlova,J. and Vorlickova,M. (2009) Arrangements of human telomere DNA quadruplex in physiologically relevant K^+ solutions. *Nucleic Acids Res.*, **37**, 6625–6634.
56. Hatters,D.M., Wilson,L., Atcliffe,B.W., Mulhern,T.D., Guzzo-Pernell,N. and Howlett,G.J. (2001) Sedimentation analysis of novel DNA structures formed by homo-oligonucleotides. *Biophys. J.*, **81**, 371–381.
57. Li,J., Correia,J.J., Wang,L., Trent,J.O. and Chaires,J.B. (2005) Not so crystal clear: the structure of the human telomere G-quadruplex in solution differs from that present in a crystal. *Nucleic Acids Res.*, **33**, 4649–4659.
58. Bugaut,A. and Balasubramanian,S. (2008) A sequence-independent study of the influence of short loop lengths on the stability and topology of intramolecular DNA G-quadruplexes. *Biochemistry*, **47**, 689–697.
59. Smargiasso,N., Rosu,F., Hsia,W., Colson,P., Baker,E.S., Bowers,M.T., De Pauw,E. and Gabelica,V. (2008) G-quadruplex DNA assemblies: loop length, cation identity, and multimer formation. *J. Am. Chem. Soc.*, **130**, 10208–10216.